Protein Imbalance in the Development of Skeletal Muscle Wasting in Tumor-Bearing Mice.

Jacob L. Brown[1], David E. Lee[1], Megan E. Rosa-Caldwell[1], Lemuel A. Brown[2,3], Richard A. Perry[2], Wesley S. Haynie[2], Kendra Huseman[4], Kavithalakshmi Sataranatarajan[4], Holly Van Remmen[4], Tyrone A. Washington[2], Michael P. Wiggs[5*], Nicholas P. Greene[1*]

*Corresponding authors

[1] Integrative Muscle Metabolism Laboratory, Exercise Science Research Center, Department of Health, Human Performance and Recreation, University of Arkansas, Fayetteville, AR 72701

[2] Exercise Muscle Biology Laboratory, Exercise Science Research Center, Department of Health, Human Performance and Recreation, University of Arkansas, Fayetteville, AR 72701

[3]Department of Molecular and Integrative Physiology, University of Michigan, Ann Arbor, MI 48109

[4]Aging and Metabolism Research Program, Oklahoma Medical Research Foundation, 825 N.E. 13th Street, Oklahoma City, OK 73104, United States; Oklahoma City VA Medical Center, Oklahoma City, OK, United States.

[5]Integrated Physiology and Nutrition Laboratory, Department of Health and Kinesiology, University of Texas at Tyler, TX 75799

Corresponding Author: Nicholas P. Greene

Exercise Science Research Center

University of Arkansas

This is the author manuscript accepted for publication and has undergone full peer review but has not been through the copyediting, typesetting, pagination and proofreading process, which may lead to differences between this version and the Version of Record. Please cite this article as doi: 10.1002/jcsm.12354

155 Stadium Dr, 321Q HPER

Fayetteville, AR 72701

E-mail: npgreene@uark.edu

Phone: 479-575-6638

Fax: 479-575-2853

OR

Michael P. Wiggs

University of Texas at Tyler

3900 University Blvd, 2186 HPC

Tyler, TX 75799

Email: mwiggs@uttyler.edu

Phone: 903-566-7306

Fax: 903-566-7065

Running Title: Cancer cachexia induced by dysregulated protein turnover.

Abstract

Background: Cancer-cachexia occurs in approximately 80 percent of cancer patients and is a key contributor to cancer-related death. The mechanisms controlling development of tumor-induced muscle wasting are not fully elucidated. Specifically, the progression and development of cancer-cachexia is underexplored. Therefore, we examined skeletal muscle protein turnover throughout the development of cancer-cachexia in tumor-bearing mice.

Methods: Lewis Lung Carcinoma (LLC) was injected into the hind-flank of C57BL6/J mice at 8 wks age with tumor allowed to develop for 1, 2, 3, or 4 wks and compared to PBS injected control. Muscle size was measured by cross sectional area analysis of Hematoxylin and Eosin stained Tibialis Anterior Muscle. $^{2}H_2O$ was used to assess protein synthesis throughout the development of cancer-cachexia. Immunoblot and rt-qPCR were used to measure regulators of protein turnover. TUNEL staining was utilized to measure apoptotic nuclei. LLC Conditioned Media (LCM) treatment of C2C12 myotubes was used to analyze cancer-cachexia *in-vitro.*

Results: Muscle cross sectional area decreased ~40% 4 wks following tumor implantation. Myogenic signaling was suppressed in tumor-bearing mice as soon as 1 wk following tumor implantation, including lower mRNA contents of Pax7, MyoD, CyclinD1 and Myogenin, when compared to control animals. AchRδ and AchRε mRNA contents were down-regulated by ~50% 3 wks following tumor implantation. Mixed fractional synthesis rate (FSR) protein synthesis was ~40% lower in 4 wk tumor-bearing mice when compared to PBS controls. Protein ubiquitination

was elevated by ~50% 4wks after tumor implantation. Moreover, there was an increase in autophagy machinery after 4 wks of tumor growth. Finally, ERK and p38 MAPK phosphorylations were 4- and 3- fold greater than control muscle 4 wks following tumor implantation, respectively. Inhibition of p38 MAPK, but not ERK-MAPK, *in-vitro* partially rescued LCM-induced loss of myotube diameter.

Conclusions: Our findings work towards understanding the pathophysiological signaling in skeletal muscle in the initial development of cancer-cachexia. Shortly following the onset of the tumor-bearing state alterations in myogenic regulatory factors are apparent, suggesting early onset alterations in the capacity for myogenic induction. Cancer-cachexia presents with a combination of a loss of protein synthesis and increased markers of protein breakdown, specifically in the ubiquitin-proteasome system. Also, p38 MAPK may be a potential therapeutic target to combat cancer-cachexia via a p38-FOX01-atrogene-ubiquitin proteasome mechanism.

Key Words: protein synthesis, LLC, ubiquitin, MAPK, ERK, p38

Introduction

Cancer is one of the leading causes of death worldwide with over half of the people affected by cancer dying as a result of the condition (1, 2). Cancer-cachexia is a wasting syndrome that occurs in approximately 80% of cancer patients (3-5). In fact, cancer-cachexia is the primary cause of death for 20%-40% of cancer deaths (3-5). Cancer-cachexia is defined as a multifactorial syndrome which displays an ongoing loss of skeletal muscle mass (with or without loss of fat mass) that cannot be fully reversed by conventional nutritional support and leads to progressive functional impairment (3, 5). As efforts to reverse cancer-cachexia have been largely unsuccessful, recent suggestions in the literature have emphasized needs to focus on prevention of the condition (6). However, few efforts have been placed toward understanding the early stage development of cancer-cachexia. We recently demonstrated that multiple measures of muscle mitochondrial health are impaired well before onset of measurable muscle wasting in cancer-cachexia in Lewis Lung Carcinoma (LLC) tumor-bearing mice beginning with increased mitochondrial ROS emission, followed by network degeneration and eventual decrements in respiratory function using this same time course model (7). Those data suggest early onset derangements in muscle health. However, skeletal muscle atrophy occurs primarily by an imbalance of protein turnover favoring protein degradation over protein synthesis (8, 9). Therefore, a critical need remains to define alteration of muscle protein turnover processes in the initial development of cancer-cachexia induced muscle wasting.

From prior literature, it is clear cancer-cachexia is associated with decreased rates of muscle protein synthesis, and increased rates of protein degradation (10-13). We also know that protein turnover is regulated by a series of anabolic processes including myogenesis and protein synthesis (10-22), and catabolic processes including the ubiquitin proteasome system, autophagy, and apoptosis (8, 13, 23-28). Each of these processes may present significant dysregulation during cancer-cachexia; however, the nature by which this negative protein balance initially develops in cancer-cachexia remains largely unknown. The initial development of cancer-induced muscle wasting is understudied in scientific literature despite the need to consider measures to prevent the condition. To this point, other prior studies have examined progression of cancer-cachexia (15, 29), though in most cases focus is placed on varying degrees of cachexia rather than the initial onset of muscle loss. In fact, a prior study by White et al. (15) previously demonstrated, a clear and progressive reduction in protein synthesis and induction of protein ubiquitination with worsening of cachexia. However, in their work efforts were focused on progression through worsening cachexia and did not examine protein turnover and other anabolic/catabolic processes in the pre-wasting state as compared to healthy control. Therefore, the purpose of this study was to examine regulation of protein turnover in skeletal muscle throughout a time course progression of cancer-cachexia in tumor-bearing mice. By examining a comprehensive measurement of protein turnover regulation throughout the progression of cancer-cachexia we provide key information about the pathogenesis of this condition. In doing so, we identified that the onset of negative protein balance and muscle wasting is met with the

induction of MAPK systems. Therefore, to determine the potential of targeting MAPKs in preventive efforts to cachectic wasting, we used LLC Conditioned Media (LCM) to mimic cancer-cachexia *in-vitro*, combined with inhibitors specific to p38 and MEK (upstream of ERK MAPK) (30, 31). The data presented herein present novel insight to the onset of the negative protein balance in cancer-cachexia and provide evidence for potential therapeutic targets to prevent cancer-induced muscle wasting.

Methods

Animals and Interventions

Animal experiments were performed at the University of Arkansas, Fayetteville. All procedures were approved by the Institutional Animal Care and Use Committee of the University of Arkansas. We have previously reported on several aspects regarding body and tissue masses and mitochondrial health in these same animals (7).

Tumor Implantation and Tissue Collection.

Male C57BL/6J mice were purchased from Jackson Laboratories. The mice were kept on a 12:12-h light-dark cycle with *ad libitum* access to normal rodent chow and water. $1X10^6$ LLC cells suspended in sterile PBS were implanted subcutaneously to the hind flank of mice at 8 weeks of age (7). The tumor was allowed to develop for 1, 2, 3 or 4 weeks as previously described (7). For control, a cohort of animals was given an injection of equal volume sterile PBS at 8 weeks of age and then age-matched to 4 week tumor-bearing mice at time of harvest (12 weeks of age). Animals were not fasted at time of tissue collection. To allow measure of protein synthesis, a bolus of deuterium oxide (~20 μL/g body weight) was injected intraperitoneally in the mouse approximately 24 hours before tissue collection. Drinking water was thereafter supplemented with deuterium oxide (4% deuterium oxide drinking water) in order to maintain the plasma pool of deuterium oxide (32-34). Animal tissues were quickly collected

under isoflurane anesthesia prior to euthanasia. Tissues were quickly weighed, enrichment time noted and snap-frozen in liquid nitrogen for further processing and stored at -80°C.

Histology

Tibialis Anterior (TA) muscles were imbedded in optimal cutting temperature (OCT) compound and frozen for sectioning. Sections were cut at 10 μm using a Leica CM1859 cryostat (Leica Biosystems, Buffalo Grove, IL) and stained with Hematoxylin & Eosin (H & E) for cross sectional area analysis. Muscle fibers were circled using Nikon Basic Research Imaging Software (Melville, NY). Roche Diagnostics (Indianapolis, IN) *In Situ* cell death detection Fluorescein (11684795910) was used to detect damaged DNA. Manufacturer's protocols were used. Slides were mounted with fluorescent mounting media with DAPI (ProLong Gold antifade reagent with DAPI, Invitrogen P36931). Nikon Ti-S inverted epiflourescent microscope with LED-based light source was used to image total nuclei (DAPI) and TUNEL + nuclei (FITC). Total nuclei and TUNEL + nuclei were then counted using Nikon Basic Research Imaging Software.

24-Hour Protein Synthesis In-Vivo

A detailed description of this method for measuring protein synthesis has previously been published (35). 15 mg and 35 mg of gastrocnemius muscle were powdered and homogenized in a 10% TCA solution for mixed and myofibrillar FSR, respectively. In order to isolate the

myofibrillar fraction, homogenate was centrifuged at 600 x G for 15 minutes. The supernatant containing cytosolic proteins was then discarded. Mixed and myofibrillar fractions were then washed 3 times with 10% TCA solution by centrifugation to eliminate cytosolic amino acids. Proteins were placed in 6 M HCL at 100˚C hydrolyze proteins into amino acids. An aliquot of the hydrolysate was dried down and derivatized with a 3:2:1 v/v solution of methyl-8, methanol, and acetonitrile to determine ^{2}H-labeling of alanine on its methyl-8 derivative. The solution was then placed in a GC-MS capillary column (Agilent 7890A GC HP-5 ms capillary column) and positioned in the GC-MS. 1 µL of solution was ran on the Agilent GC-MS at an 80:1 split. GC-MS settings have previously been described (33, 35). A ratio of deuterated alanine over alanine was employed to assess protein synthesis.

The precursory pool of ^{2}H2O in the plasma was reacted with 10 M NaOH and a 5% solution of acetone in acetonitrile for 24 h in order to conjugate the free ^{2}H2O to acetone. The solution was extracted by adding Na_2SO_4 and chloroform, and placed in capillary columns to be analyzed on the GC-MS to detect acetone at an 80:1 split.

FSR of mixed and myofibrillar proteins were calculated using the equation EA × [EBW × 3.7 × t (h)]−1 × 100, where EA represents amount of protein-bound [2H]alanine (mole% excess), EBW is the quantity of ^{2}H2O in body water (mole% excess), 3.7 represents the exchange of ^{2}H between body water and alanine (3.7 of 4 carbon-bound hydrogens of alanine exchange with water) and t(h) represents the time the label was present in hours.

RNA isolation, cDNA synthesis, and quantitative real-time PCR

Adult gastrocnemius muscles were collected and frozen in liquid nitrogen at time of harvest. 20-30 µg of powdered gastrocnemius muscle was homogenized into a 1 mL TRIZOL solution, and RNA was isolated using a commercially available kit (Ambion, Life Technologies). Isolated RNA purity and concentration was confirmed using Bio-Tek (Winooski, VT) Power Wave XS plate reader with Take3 microvolume plate and Gen5 software. After which, 1 µg of RNA was reverse transcribed into cDNA using previously described methods and Vilo SuperScript (11755050, Invitrogen, Carlsbad, CA) reagents cDNA was diluted to 1:100 (10 ng/µL) and Ct values analyzed using TaqMan reagents and commercial Step-One real-time RT-PCR instrumentation (Applied BioSystems, Foster City, CA). Assessment of 18s (Mm03928990_g1), *Pax7* (Mm01354484_m1), *MyoD* (Mm00440387_m1), *MyoG* (Mm00446194_m1) *Atrogin1* (Mm00499523_m1), *MuRF1* (Mm01185221_m1) and *Cyclin D1* (Mm00432359_m1) were performed using TaqMan probes (Life Technologies) and corresponding TaqMan reagents. No differences were seen in 18s among experimental conditions for experiments presented. Final quantification of gene expression was calculated using the ΔΔCT method. Relative quantification was calculated as $2^{-\Delta\Delta CT}$.

Immunoblotting

Gastrocnemius muscle was homogenized in a buffer containing 0.23 M Tris-HCL, pH 6.8, 4.5% w/v SDS, 45% glycerol, 0.04% w/v Bromophenol Blue, 80 mM dithiothreitol,

0.57mM 2-mercaptoethanol, complete, mini protease inhibitor cocktail (Roche, Indianapolis, IN), and phosphatase inhibitor cocktails (Sigma-Aldrich) and denatured at 95°C. Concentrations were determined using the RC/DC assay (500-0119, BioRad, Hercules, CA) and 40 μg total protein was resolved by SDS-PAGE, transferred to a PVDF membrane and blocked in 3% w/v Bovine Serum Albumin in Tris-buffered saline with 0.2% Tween 20 (TBST). Membranes were probed overnight for primary antibodies specific to p-AKT (Cell Signaling 9271, S 473), AKT (Cell Signaling 9272), Deptor (EMDMillipore, ABS222), p-4EBP1 (Cell Signaling 9451 S 65), 4EBP1 (Cell Signaling 9452), p-p70s6k (Cell Signaling 9205, T 389), p70s6k (Cell Signaling 9202), p-FOXO1 (Cell Signaling 9464, T24), FOXO1 (Cell Signaling 2880), p-FOXO3 (Cell Signaling 9464, T32), FOXO3 (Cell Signaling 2497), p-FOXO4 (Cell Signaling 9471, S 197), FOXO4 (Cell Signaling 9472), Ubiquitin (Cell Signaling 3933), Beclin1 (Cell Signaling 3738), p62 (Sigma p0067), LC3 (Cell Signaling 4108), Caspase 3 (Cell Signaling 9662), ERK 1/2 MAPK (Cell Signaling 4695), p-ERK 1/2 MAPK (Cell Signaling 4370, T 202/ Y204), p-p38 MAPK (Cell Signaling 9211, T 180/182), p38 MAPK (Cell Signaling 9212), p-MAPK APK (Cell Signaling 3316S, T 222) and MAPK APK (Cell Signaling (3042S) isolated from rabbit and mouse. Antibodies were diluted in TBST with 5% milk. LiCor secondary antibodies conjugated with HRP (animal experiments) or Infared (IR) Dye (cell culture experiments) were used according to manufacturer's protocols. For animal experiments, membranes were imaged on Protein Simple FluorChem (Minneapolis, MN) with LiCor WesternSure Premium Chemiluminescent substrate (926-95000) and analyzed using Alpha View software. For cell

culture experiments membranes were imaged on LiCor Odyssey FC using IR detection. All bands were normalized to the 45 kDa Actin band of Ponceau S stain as a loading control.

Cell Culture Experiments

C2C12 myoblasts were plated at 50,000 cells per well of a 6 well cell culture plate with 2 mL DMEM (11965092, Life Technologies, Carlsbad, CA) supplemented with 20% Fetal Bovine Serum (26140079, Life Technologies) and 1% pen/strep (15140122, Life Technologies) as per previous work by us (36, 37) and others (38). Cell proliferation and differentiation were performed as previously described (36, 37), briefly, at confluence media was switched to DMEM supplemented with 2% horse serum, 1% P/S, 50% HEPES, 0.75% transferrin and 0.75% insulin for 5 days. Myoblasts were plated for experiments at passage 6.

LLC Conditioned Media Treatment

In order to collect LLC conditioned media (LCM), LLC cells were grown to 100% confluence as previously described (7, 39). LLC cells were then incubated in DMEM supplemented with 10% Fetal Bovine Serum and 1% pen/strep for 18 hours. The media was then collected and filtered. LLC conditioned media was then diluted to 25% total volume in serum free media. For the Control group, 25% total volume of 10% fetal bovine serum growth media was diluted in serum free media. C2C12 myotubes were then treated with either control or LCM for 24 hours. This method was adapted from Puppa et al. (16) and Guohua et al. (31). Dilution of conditioned media should reduce effects of nutrient deprivation following the incubation period.

Notably, recent works show that both conditioned media and co-culture with tumor cells (C26) induce myotube atrophy (40) and thus effects described herein are believed to be due to tumor-derived factors rather than nutrient deprivation.

Inhibition of p38 and ERK 1/2 MAPKs

To examine the roles of p38 MAPK and ERK 1/2 MAPK in the loss of myotube diameter on the on myotubes treated with Control or LCM, differentiated C2C12 myotubes were treated with PD098059 (20 μM; PHZ1164, Life Technologies) (MEK1/2 inhibitor preventing ERK 1/2 activity) or SB202190 (20 μM; S7067, Sigma Aldrich) (inhibitor of p38 MAP kinase) for the entire duration of control or LCM treatment. These concentrations of inhibitors have been previously published by Brown et al. (36).

C2C12 Myotube Protein and RNA Collection

After LCM and drug treatment experiments, myotubes were collected for immunoblot and RNA isolation by applying 100 μL of 2X protein sample buffer or 1 mL of TRIZOL, respectively. Subsequent steps were performed as described above.

Myotube Diameter Analysis

Myotube diameter analysis was performed as previously published (36, 37). Briefly, C2C12 myoblasts proliferated until 80-100% confluency. The myoblasts were differentiated for 120 hours. Myotubes were then placed in control or LCM and appropriate drug treatments were

added. Myotubes were imaged with a 40X objective with 10 images per well and 3-4 myotubes examined per well. 5 lines were drawn across the diameter of each myotube in order to measure the average diameter of the myotube. This was performed on every myotube imaged in the experimental conditions. Researcher was blinded for this analysis. A second researcher then repeated experiments with images acquired using a 10X objective and measurements as described above. All cell culture experiments were conducted in triplicate and repeated in order to ensure data accuracy.

SuNSET Protein Synthesis

Protein synthesis in tissue culture was measured using the SuNSET protocol (41, 42) as we have previously published (37). Briefly, 1 μM puromycin dihydrochloride (Calbiochem, Darmstadt, Germany) was added to cell culture media and incubated 30 minutes prior to protein extraction. Immunoblotting protocols were followed as described above using 1:20,000 dilution of mouse anti-puromycin IgG 2a antibody (EMD Millipore, Darmstadt, Germany) followed by 1:20,000 dilution of HRP conjugated anti-mouse IgG fragment specific 2a antibody (Jackson ImmunoResearch Labs, West Grove, PA). The entire lane was assessed for optical density and this was normalized to optical density of the entire lane of Ponceau S stain. This was used as a relative measure of the amount of actively translated proteins in the polysome prior to harvest of cells.

Statistical Analysis

For animal experiments, independent factors were PBS and number of weeks tumor progressed. A One-Way ANOVA was employed as the global analysis for each dependent variable. For cell culture experiments, independent factors included media (con or LCM) and drug treatment (Vehicle or SB202190/PD98059 as appropriate to experiment). These independent factors were divided into two separate cell culture experiments herein referred to as LCM p38 inhibitor and LCM ERK 1/2 inhibitor. Data in each separate cell culture experiments were analyzed by two-way ANOVA with factors of media (Con vs LCM) and pharmacological inhibition (Vehicle vs SB202190 or PD98059). Where significant F-ratios were found, differences among means were determined by Student Newman-Keuls post hoc test for both the animal and cell culture experiments. For all experiments, the comparison-wise error rate, α, was set at 0.05 for all statistical tests. All data were analyzed using the Statistical Analysis System (SAS, version 9.3, Cary, NC, USA), figures were compiled using GraphPad Prism (La Jolla, CA, USA) and data expressed as mean ± SEM.

Results

Characterization of the progression of LLC-induced cancer-cachexia. We have previously reported phenotypic characteristics of these same mice including body and tissue masses (7). Most importantly, muscle wet weights were ~15-20% lower 4 wks following tumor implantation when compared to PBS control mice (7). Here, we report that mean CSA of TA muscle fibers were ~15% smaller 3 wks following tumor implantation and ~40% smaller by 4 wks of tumor growth compared to PBS control mice (Figure 1B). Furthermore, there were a

larger number of small fibers (200μM^2-600μM^2 area) and a smaller number of large fibers (>1400 μM^2) when comparing 4 wks of tumor burden to PBS control mice (Figure 1C).

Extrinsic regulators of skeletal muscle mass are impaired throughout the development of cachexia. To determine the impacts of the tumor-bearing state on anabolic functions in the muscle we assessed aspects of myogenesis and protein synthesis. Briefly, myogenesis is the formation of muscular tissue, which is necessary for repair of injured muscle. Satellite cells are labeled with Pax7 (43). Upon activation, satellite cells express MyoD and subsequently Myogenin which are responsible for proliferation and differentiation of satellite cells, respectively (21, 22). There is evidence that myogenic dysregulation may promote cancer-induced muscle wasting (20). From these assessments we observed that *Pax7* mRNA content was ~35% lower 1 wk following tumor implantation when compared to PBS control mice, and did not recover throughout the progression of cancer-cachexia (Figure 2A). *MyoD* mRNA content was ~50% lower in both 1 wk and 2 wk tumor-bearing groups when compared to PBS control mice (Figure 2A). mRNA content of *MyoD* recovered 3 wks following tumor implantation. In tumor-bearing mice, *CyclinD1* mRNA content was ~45% lower than PBS control mice in all tumor-bearing groups (Figure 2A). *Myogenin* mRNA was ~50% lower than PBS control mice 1 wk following tumor implantation, but recovered by 3 and 4 wks following tumor implantation (Figure 2A). Finally, we assessed mRNA content of putative markers of muscle denervation. We observed that while mRNA of Acetylcholine Receptor (AchR) α, Gad45A, RUNX1 and MusA were not significantly altered (Figure S1). AchR δ and AchR ε

were downregulated by ~35% and 45% 2 wks and 3 wks following tumor implantation, respectively (Figure S1).

Mixed protein synthetic rate is lower in cachectic muscle. Next, in our assessment of anabolic function we determined 24-h FSR and assessed mTOR signaling components. Mixed muscle FSR was ~40% lower than the PBS control group 4 wks following tumor implantation with no other significant differences among experimental conditions (Figure 3A). In contrast, there was no significant change in myofibillar FSR during the progression of cancer-cachexia (Figure 3B); however, there was a mean decrease in the 3 and 4 wk groups when compared to PBS ($p=0.3$). To examine mTOR related signaling we assessed the upstream marker Akt, mTOR Complex component and negative regulator of mTOR – Deptor, and downstream mTOR targets p70S6K1 and 4EBP-1 (17, 18) (44). We observed that content and phosphorylation of Akt, p70s6k and 4EBP1 did not change throughout the progression of cancer-cachexia (Figure 3C). However, Deptor protein content was ~40% greater 3 wks following tumor implantation when compared to other experimental groups (Figure 3C).

Protein breakdown is upregulated in cachectic muscle. To investigate the contributions of putative catabolic processes we assessed markers of the ubiquitin-proteasome system, autophagy and apoptosis. With regards to the ubiquitin-proteasome system, FOXO1 and FOXO3 signaling are important regulators of the atrogenes: Atrogin1 and MuRF1 (23). These are important E3 ligases known to promote skeletal muscle wasting (23). Muscle protein ubiquitination was ~50% higher than PBS control mice 4 wks following tumor implantation

(Figure 4A). We observed that total FOXO1 protein content was ~50% greater than PBS control mice 4 wks following tumor implantation (Figure 4A). Phosphorylation status of FOXO3^{T32} and FOXO4^{T28} did not change as tumor growth progressed; however, there was a non-significant mean decrease in relative FOXO1^{T24} phosphorylation (Figure 4A). Furthermore, *Atrogin1* mRNA content was 3 fold greater than PBS control mice 4 wks after tumor implantation (Figure 4B), while MuRF1 mRNA content was 2 and 4 fold greater than PBS control mice at 3 and 4 wks following tumor implantation (Figure 4B), respectively.

To provide insight into the potential contributions of autophagy, a process involved in the formation of an autophagosome in order to facilitate lysosomal clearance of proteins and organelles (26-28), we examined upstream regulator Beclin1, as well as LC3 (involved in the closing of the autophagosome) and p62 (a linker protein between the autophagosome and cargo that is degraded by the lysosome upon completion of autophagy). Beclin1 protein content was ~80% greater than PBS control mice 4 wks post tumor implantation (Figure 4C). Furthermore, total LC3 protein content was ~60% higher than PBS control mice after 4 wks of tumor growth (Figure 4C). By contrast, there was no difference in the LC3 II:I ratio throughout the progression of cancer-cachexia (Figure 4C) nor in protein content of p62 (Figure 4C).

Apoptosis is not altered in progression of LLC-induced cancer-cachexia. To examine apoptosis in cachectic muscle, we used TUNEL staining, and Caspase 3 protein content. Loss of myonuclei may limit the muscles' ability to increase in size. There was no significant difference in the number of TUNEL positive nuclei throughout the progression of cancer-cachexia (Figure

5A). Moreover, total Caspase 3 was not different between the PBS, 1 wk, 2 wk, 3 wk and 4wk groups (Figure 5B) while Cleaved Caspase 3 (active form) was not detectable by immunoblot.

MAPK phosphorylation is induced in tumor-bearing mice. MAPKs are key controllers of both anabolic and catabolic signaling within skeletal muscle (45, 46), therefore in order to assess MAPKs in cachectic muscle we examined p38 and ERK phosphorylation status. $ERK^{T202/Y204}$ and $p38^{T180/Y182}$ MAPK phosphorylations relative to respective total protein contents were 4 fold and 3 fold greater than PBS control mice 4 wks following tumor implantation, respectively (Figure 6A/B).

ERK 1/2 Inhibition does not protect against LCM-mediated loss of myotube diameter despite promoting protein synthesis. Considering that induction of MAPK phosphorylation occurs concurrent with the development of muscle wasting in the current study, and the induction of a negative protein balance, we elected to examine MAPKs role in the development of cancer-cachexia *in-vitro.* To do so, we used LCM treatment of C2C12 myotubes to mimic cancer-cachexia, and appropriate selective MAPK inhibitors for each experiment. First, to test whether ERK MAPK inhibition could protect against LCM-induced myotube atrophy, myotubes were concurrently treated with PD98059. In these experiments, diameter of myotubes treated with LCM was ~35% lower than the diameter of myotubes treated with Control media, and was not affected by the addition of PD98059 (Figure 7A). LCM loss of myotube diameter was similar to the loss of muscle mass observed *in-vivo* (40% loss in CSA *in vivo*, 35% loss in myotube diameter *in vitro*). Phosphorylated ERK relative to total ERK was ~50% lower in groups

containing PD98059 when compared to the Control Media+Vehicle group (Figure 7B). Also, ERK phosphorylation in LCM+Vehicle was ~50% lower than Control+Vehicle (Figure 7B). Puromycin incorporation was 3 fold and 2 fold greater in Control+PD98059 and LCM+PD98059, respectively when compared to Control+Vehicle (Figure 7C). Protein ubiquitination in LCM treated conditions were ~40% greater than control media (Figure 7D). Protein content of p-4EBP1, 4EBP1, Deptor, p-FOXO3, FOXO3, p-FOXO1 and FOXO1 was not different between all groups (Figure 7E). *Atrogin-1* and *MuRF-1* mRNA content was ~25% and 35% lower in LCM+Vehicle when compared to Control+Vehicle, respectively (Figure 7F).

Inhibition of p38 MAPK partially protects against LCM-Mediated Loss of Myotube Diameter. Myotube diameter of cells treated with LCM+Vehicle was ~45% smaller than cells treated with Control Media, while myotube diameter of cells treated with LCM+SB202190 was ~25% smaller than myotubes treated with control media and ~20% greater when compared to myotube diameter of cells treated with LCM+Vehicle (Figure 8A). LCM loss of myotube diameter was similar to the loss of muscle mass observed *in-vivo*. Relative phosphorylation of MAPKAPK-2, a direct target of p38 MAPK, was ~40 and 50% in Control+ SB202190 and LCM+ SB202190 when compared to control vehicle, respectively (Figure 8B). Puromycin incorporation was ~2 fold greater in myotubes treated with SB202190 when compared to myotubes treated with vehicle, regardless of LCM treatment (Figure 8C). Protein ubiquitination was ~2 fold greater in LCM+Vehicle when compared to all other groups (Figure 8D). Protein content of p-4EBP1, 4EBP1, Deptor, p-FOXO3 and FOXO3 was not different between all

groups; however, protein content of p-FOXO1 relative to total FOXO1 was significantly elevated in LCM+Vehicle when compared to all other groups (Figure 8E). *Atrogin-1* mRNA was ~45% greater than control media groups using LCM+Vehicle treatment and ~60% lower than control media groups using LCM+SB202190 treatment (Figure 8F). *MuRF-1* mRNA was ~70% lower in groups containing SB202190 when compared with vehicle treatment (Figure 8F).

Discussion

Loss of muscle mass occurs largely from an imbalance of protein turnover favoring protein degradation (47), which is commonly observed in late stage cancer-cachexia (10, 11, 48); however, we are the first to measure modalities of protein turnover throughout a time course of the initial development of LLC-induced cancer-cachexia. In this same cohort of animals, we recently demonstrated that impaired mitochondrial health develops well prior to onset of muscle wasting (7). Those data thus suggest impaired myocellular health prior to measurable muscle wasting. Here, we have shown alterations in cellular programing necessary for the maintenance of muscle mass as soon as 1 wk following tumor implantation with impaired signaling for satellite cell proliferation and myogenesis. Interestingly, through additional assessments of muscle protein synthesis and degradative pathways including autophagy, ubiquitin-proteasome system and apoptosis, it appears primary decrements contributing to the negative protein balance occur via activation of the ubiquitin-proteasome system and reduced mixed muscle protein synthesis which develop concurrent to the onset of phenotypic muscle wasting (by muscle mass). Furthermore, upstream signaling suggests this may be mediated via activation of MAPK signaling cascades. In fact, *in vitro* inhibition of p38 MAPK blunted myotube atrophy in response to LCM. The search for efficacious treatments for cancer-induced muscle wasting is ongoing as many attempted therapeutic modalities have yielded minimal effect (49). The data presented in this study provides a comprehensive overview of machinery responsible for the

maintenance of muscle mass throughout the development of cancer-cachexia in tumor-bearing mice.

Cross Sectional Area is altered in tumor-bearing mice. In the current study cachectic muscle mass loss developed at 4 wks post tumor implantation (7), which is commonly observed in this model (7, 16, 39, 50). At 4 wks these mice display a degree of muscle mass loss (~15% smaller muscle wet weights (7), and a ~40% decrease in mean CSA) that would be considered a negative prognosis clinically and greatly increase mortality among cancer patients. We do note that CSA was reduced ~15% at 3 wks post tumor implantation despite a lack of measurable change in total muscle mass. However, the reductions in total muscle mass are smaller than many prior reports and without significant loss in tumor free body mass suggesting that 4 wk tumor-bearing mice displayed mild/moderate cachexia.

Extrinsic Regulation of Skeletal Muscle Mass. In cancer-cachexia, the sarcolemma becomes damaged due to factors secreted by the tumor, which elicits a repair response (19). Our data indicates *Pax7* mRNA, a satellite cell marker, content decreased as soon as 1 wk following tumor implantation, implying the satellite cell pool may be diminished thus impairing regenerative capacity shortly after the onset of the tumor-bearing state (51). Intriguingly, these results appear to contradict findings from He et al. (20) in which an increase in Pax7 protein content was noted in response to tumor burden in both C26 and LLC models of cancer-cachexia. These contradictions may be due to methodology differences to measure Pax7 expression. It is possible that reduced *Pax7* mRNA here coupled with increased Pax7 protein previously reported

(20) indicates altered turnover of Pax7 and accumulation of dysfunctional satellite cells, at current though this speculation requires further testing to resolve. Moreover, our data shows that MyoD (important for satellite cell proliferation (22)), MyoG (important for satellite cell differentiation (22)) and Cyclin D1 mRNA contents are decreased 1 wk following tumor implantation. This dysregulation of *MyoD* and *MyoG* mRNA expression corroborates recent findings outlining impaired myogenesis in response to tumor burden in mice (20). These data strongly suggest a defect in myogenic regulation which develops shortly following onset of the tumor-bearing condition and thus an early development in this anabolic process. Interestingly, in our prior measures of mitochondrial degeneration the primary defect therein at this early timepoint was an enhanced mitochondrial ROS emission (7). These combined data suggest in the early tumor-bearing state initial defects in myogenic regulation and mitochondrial ROS emission though at this time it is too early to state if these alterations are impacting one another. The currently assessed aberrant myogenic signaling suggests a potential limit on muscle regrowth potential that develops shortly after onset of the tumor-bearing state. Prior findings have suggested that satellite cell proliferation is not necessary for muscle regrowth (52, 53), however, most of these findings are in conditions where myonuclei may not be compromised. We have seen here that in this earlier state of cancer-cachexia apoptosis is not heavily induced, this observation is likely tied to attempts to preserve myonuclei in conditions where the satellite cell pool is compromised which may then limit muscle regrowth potential following loss of myonuclei. This effect may then limit efficacy of therapies aimed to reverse cachexia post cancer

treatment, thereby suggesting a need to determine mechanisms impairing myogenic potential in early tumor-bearing states to prevent/reverse this effect.

Interestingly, we observed a rebound in the contents of the myogenic regulatory factors MyoD and myogenin at 3 and 4 weeks post-tumor implantation. We cannot be certain as to the mechanism for this, however, these specific myogenic regulatory factors have previously been demonstrated to be elevated during denervation (54-56). Therefore, we assessed a panel of denervation markers. To that end, we have demonstrated that *AchR* δ and ε are downregulated in cachectic muscle; however, at this point we cannot conclude that functional denervation is occurring. In fact, AChR density is often higher than needed for efficient capture of the acetylcholine released at the neuromuscular junction (57); therefore, based on current data functional denervation is not likely occurring at this stage in the development of cancer-cachexia. Therefore, the mechanism for the rebound effect in MyoD and myogenin remains elusive. However, we should caution that further studies into more severe cachectic states may be necessary to determine impacts on functional denervation.

Mixed muscle protein synthesis is reduced concurrent to onset of muscle wasting in tumor-bearing mice. In cancer-cachexia literature, there is an ongoing debate as to whether a decrease in protein synthesis, upregulated protein degradation or both play a greater role in the onset of cancer-induced muscle wasting (58). There appear to be discrepancies based on both the type of model used and the methodology for measuring protein synthesis (16, 48, 58-60). Our protein synthesis data showed a decrease in the mixed muscle fraction with no significant change

in the myofibrillar fraction (despite a ~25% mean decrease in FSR) measured over a 24 hour time period. These results corroborate studies such as Toledo et al. (59) which describes a ~50% reduction in mixed protein synthesis in the gastrocnemius muscle in LLC tumor bearing mice. We are the first to measure protein synthesis in LLC tumor-bearing mice utilizing deuterium oxide for a 24 hour time period, a validated measurement of protein synthesis (32). Typically in cancer-cachexia literature protein synthetic rates have been examined in shorter time periods (16, 48, 58-61) . Our approach, may provide a specific advantage in the ability to assess protein synthetic function over the course of a full light/dark cycle and thus a potentially more accurate reflection of protein synthetic rates. In regards to myofibrillar protein synthesis, we should note that most reports measuring muscle protein synthesis in a cachectic phenotype utilize conditions with more severe wasting and concomitant greater losses in muscle and total body masses than this study (15, 16, 59, 62). It is likely that development of a more severe phenotype would alter protein synthetic signaling and induce a more severe loss of myofibrillar FSR comparable to other studies. These data suggest that decrements in mixed-muscle protein synthesis are a significant contributor to muscle wasting in LLC tumor-bearing mice.

Induction of skeletal muscle protein degradation systems in tumor-bearing mice. Our data indicates that there is increased protein breakdown 4 wks after tumor implantation. We note upregulation of E3 ligases *Atrogin1* and *MuRF1* 4 wks following tumor implantation with concomitantly significantly increased protein ubiquitination. This increase in the ubiquitin-

proteasome system likely occurs through enhanced FOXO1 content, which is responsible for promoting the expression of atrogenes such as Atrogin1 and MuRF1 (63-65).

Autophagy is another key controller of protein breakdown (26-28). Our data indicates an increase in Beclin1 and LC3 protein content 4 wks following tumor-implantation. Based on current data it appears that basal rates of autophagy are not significantly affected (lack of change in LC3II:I ratio and p62 content) in the cachectic state; however, autophagy machinery (Beclin1 and LC3) appears to be upregulated suggesting greater capacity for protein degradation through this system in cachectic muscle. Finally, as discussed above in relation to the regulation of myonuclei, we observed no significant induction of apoptosis in the muscle of cachectic mice, suggesting that at this stage of mild/moderate cachectic wasting apoptosis is not a primary contributor to muscle catabolism. However, we cannot, based on our data, rule out that apoptosis may play a more prominent role in muscle losses as the degree of cachexia becomes more severe. In that situation the concomitant impairments in myogenic regulation we have observed may become more critical in muscle regrowth and recovery.

Therefore, in our assessments of muscle anabolic and catabolic functions in tumor-bearing mice we observe early onset decrements to myogenic signaling, followed by reduced mixed muscle protein synthesis, increased ubiquitin-proteasome function, and an upregulation of autophagy machinery. Prior studies of protein turnover with progression of cancer-cachexia have largely focused on the worsening of the cachectic state itself (15). In those works it is apparent that negative protein balance becomes further exacerbated with the overall condition in greater

decrements of protein synthesis and inductions of catabolic systems. Combined with present findings we now see that negative protein balance (reduced synthesis and enhanced breakdown) occurs concomitant with the onset of muscle loss regardless of body mass losses. Loss of protein synthesis and the promotion of protein breakdown occur concomitantly with the onset of cancer-mediated muscle loss.

MAPK signaling is altered in tumor-bearing mice. To identify potential signaling mechanisms leading to impaired protein anabolism and enhanced protein breakdown we next examined MAPK signaling in tumor-bearing mice. Our data shows that both ERK and p38 MAPK phosphorylation's increase by 4 fold and 3 fold, respectively concurrent with the negative protein balance observed in this study. Prior literature shows that an increased phosphorylation, and corresponding activation, of these MAPKs can lead to both impaired muscle regeneration and increased protein breakdown (45, 46, 66-70). In order to examine MAPKs role in promoting cancer-cachexia, we subsequently elected to use LLC-conditioned media, a well-established model to mimic tumor-mediated muscle wasting *in-vitro* (30, 31). We observed a partial rescue of tumor-mediated loss of myotube diameter by inhibiting p38 MAPK, with no effect of ERK MAPK on LCM-induced myotube atrophy. Long term (~18 hours) p38 inhibition appeared to prevent tumor derived catabolism (protected against LCM-induced protein ubiquitination and upregulation of *Atrogin1*) and promoted protein synthesis. Of note, long term inhibition of both p38 and ERK MAPK stimulated protein synthesis *in-vitro* regardless of LCM treatment. However, it is interesting to note that while ERK MAPK inhibition promoted protein

synthesis it did not protect against LCM-induced atrophy suggesting that p38 MAPK's inhibition of protein ubiquitination and atrogenes (likely independent of FOXO regulation) were likely key to protect from LCM-induced atrophy. We do note as a limitation in the current experiment that we were unable to detect induction of p38 and ERK MAPK phophorylations *in vitro*. We should note however, that prior similar experiments have observed induced p38 and ERK MAPK phosphorylation following LCM treatment 72h LCM treatment (30) suggesting that detection of these inductions may require a longer time period of exposure and thus we expect here that timing of our assessments may have prevented us from being able to measure induced activation of these MAPKs. The authors find it interesting to note that 72h course of exposure to LCM (30) compared to the 24h exposure here may be necessary to detect induction of p38 and ERK phosphorylations with the LCM model is consistent with our *in vivo* evidence in which these alterations are not apparent until later in the development of LLC-induced muscle atrophy. While at this point we cannot determine whether inhibition of MAPK protects adult skeletal muscle from tumor-mediated wasting *in-vivo*; these data provide a promising potential mechanism for the onset of cachectic muscle wasting via p38 MAPK phosphorylation. In fact, recent evidence suggests that p38 MAPK blockade, or deletion of the p38β isoform in skeletal muscle, blocks Activin A induced catabolic signaling and completely protects against Activin A-induced myotube atrophy (68). Interestingly, efforts to more directly test effects of proteasomal inhibition have led to mixed results with some protection in muscle atrophy by specific targeting of MuRF1 (71) and no protection seen with the proteasome inhibitor Bortezomib (72), while growth

hormone secretagogues attenuate both induction of MuRF1 and muscle wasting (73). These data suggest the effects of p38 MAPK inhibition are likely at least in part due to protection against MuRF1-ubiquitin-proteasome induction. Overall, protection against catabolic functions, as performed here via p38 MAPK blockade, and in other studies through may be key to attenuation of cancer-induced muscle wasting (71, 74, 75). Combined with prior findings it now appears that p38 MAPK signaling may be a key regulator of cancer-induced muscle wasting. Additionally, more research is needed to elucidate the underlying mechanisms responsible for the observed stimulation of protein synthesis via long term MAPK inhibition. Our current data both *in vivo* and *in vitro* are suggestive of the importance of the catabolic p38-FOX01-atrogene-ubiquitin proteasome axis in the development of cancer-induced muscle wasting. New studies should aim to determine if inhibition of p38 MAPK *in vivo* may alleviate cancer-induced muscle wasting.

Summary and conclusions. In this study, we have analyzed muscle size, myogenesis, protein turnover and apoptosis throughout the progression of cancer-cachexia. Based on our data, loss of mixed protein synthetic rates along with increased protein breakdown via the ubiquitin-proteasome system are likely the major contributors for the onset of cancer-induced muscle wasting in LLC tumor-bearing mice which develop at the onset of muscle wasting. Furthermore, there appear to be early alterations in myogenic signaling potentially contributing to the irreversibility of cancer-cachexia. Aberrant p38 MAPK signaling is a likely major contributing factor in the onset of LLC-induced cancer-cachexia as p38 MAPK phosphorylation is induced concomitant to developments of negative protein balance and muscle loss in tumor-bearing mice

and p38 MAPK inhibition partially protected against LCM-induced myotube atrophy *in-vitro*. The search for efficacious therapeutic strategies in cancer-cachexia and other wasting disorders continues, while strategies to target various functional aspects within the muscle have had some effect (76, 77), it appears that the inhibition of catabolic systems may be key to preservation of mass. Therefore, future research should continue to examine the potential of targeting p38 MAPK and the anti-catabolic effects therein in cancer-cachexia induced muscle wasting. These data provide novel information for the mechanisms contributing to muscle atrophy and potential insight for development of therapies to prevent and treat cancer-cachexia.

Acknowledgements

Support for LLC experiments has been provided in part by the Arkansas Biosciences Institute, the major research component of the Arkansas Tobacco Settlement Proceeds Act of 2000 and National Institutes of Health under Award Number R15AR069913 from the National Institute of Arthritis And Musculoskeletal And Skin Diseases and the National Institute Of General Medical Sciences. Contents of this publication are solely the responsibility of the authors and do not necessarily represent the official views of the ABI, NIGMS or NIH. The authors would like to thank Drs. Sami Dridi, Elizabeth Greene and Jeffrey Wolchok (U. Arkansas), as well as Mr. Connor Benson (UT Tyler), Ms. Lisa Jansen, Ms. Haley McCarver and Mrs. Katie Stephenson-Brown for their contributions to the experiments presented here and editing. We would like to

thank the Cell and Molecular Biology program at the University of Arkansas, Fayetteville for supporting Jacob L. Brown's graduate education. We would also like to extend our gratitude to the numerous other faculty, Exercise Science Research Center at the University of Arkansas.

The authors certify that they comply with the ethical guidelines for publishing in the Journal of Cachexia, Sarcopenia and Muscle (78).

Conflict of Interest.

All authors declare no conflicts of interest.

References

1. Ferlay J, Soerjomataram I, Dikshit R, Eser S, Mathers C, Rebelo M, et al. Cancer incidence and mortality worldwide: sources, methods and major patterns in GLOBOCAN 2012. Int J Cancer. 2015;136(5):E359-86.

2. Fitzmaurice C, Dicker D, Pain A, Hamavid H, Moradi-Lakeh M, MacIntyre MF, et al. The Global Burden of Cancer 2013. JAMA Oncol. 2015;1(4):505-27.

3. Fearon Kenneth CH, Glass David J, Guttridge Denis C. Cancer Cachexia: Mediators, Signaling, and Metabolic Pathways. Cell Metab. 2012;16(2):153-66.

4. Onesti JK, Guttridge DC. Inflammation based regulation of cancer cachexia. Biomed Res Int. 2014;2014:168407.

5. Fearon K, Strasser F, Anker SD, Bosaeus I, Bruera E, Fainsinger RL, et al. Definition and classification of cancer cachexia: an international consensus. Lancet Oncol. 2011;12(5):489-95.

6. Fearon K. Cachexia: Treat wasting illness on multiple fronts. Nature. 2016;529(7585):156.

7. Brown JL, Rosa-Caldwell ME, Lee DE, Blackwell TA, Brown LA, Perry RA, et al. Mitochondrial degeneration precedes the development of muscle atrophy in progression of cancer cachexia in tumour-bearing mice. J Cachexia Sarcopenia Muscle. 2017.

8. Narsale AA, Puppa MJ, Hardee JP, VanderVeen BN, Enos RT, Murphy EA, et al. Short-term pyrrolidine dithiocarbamate administration attenuates cachexia-induced alterations to muscle and liver in ApcMin/+ mice. Oncotarget. 2016.

9. Oliveira AG, Gomes-Marcondes MC. Metformin treatment modulates the tumour-induced wasting effects in muscle protein metabolism minimising the cachexia in tumour-bearing rats. BMC cancer. 2016;16:418.

10. Suzuki H, Asakawa A, Amitani H, Nakamura N, Inui A. Cancer cachexia—pathophysiology and management. JGH Open. 2013;48(5):574-94.

11. Miyamoto Y, Hanna DL, Zhang W, Baba H, Lenz HJ. Molecular Pathways: Cachexia Signaling-A Targeted Approach to Cancer Treatment. Clin Cancer Res. 2016;22(16):3999-4004.

12. Tisdale MJ. The ubiquitin-proteasome pathway as a therapeutic target for muscle wasting. J Support Oncol. 2005;3(3):209-17.

13. Aversa Z, Pin F, Lucia S, Penna F, Verzaro R, Fazi M, et al. Autophagy is induced in the skeletal muscle of cachectic cancer patients. Sci Rep. 2016;6:30340.

14. White JP, Puppa MJ, Gao S, Sato S, Welle SL, Carson JA. Muscle mTORC1 suppression by IL-6 during cancer cachexia: a role for AMPK. Am J Physiol Endocrinol Metab. 2013;304(10):E1042-E52.

15. White JP, Baynes JW, Welle SL, Kostek MC, Matesic LE, Sato S, et al. The regulation of skeletal muscle protein turnover during the progression of cancer cachexia in the Apc(Min/+) mouse. PloS one. 2011;6(9):e24650.

16. Puppa MJ, Gao S, Narsale AA, Carson JA. Skeletal muscle glycoprotein 130's role in Lewis lung carcinoma-induced cachexia. FASEB J. 2014;28(2):998-1009.

17. Gingras AC, Raught B, Gygi SP, Niedzwiecka A, Miron M, Burley SK, et al. Hierarchical phosphorylation of the translation inhibitor 4E-BP1. Genes Dev. 2001;15(21):2852-64.

18. Burnett PE, Barrow RK, Cohen NA, Snyder SH, Sabatini DM. RAFT1 phosphorylation of the translational regulators p70 S6 kinase and 4E-BP1. Proc Natl Acad Sci U S A. 1998;95(4):1432-7.

19. Penna F, Costamagna D, Fanzani A, Bonelli G, Baccino FM, Costelli P. Muscle wasting and impaired myogenesis in tumor bearing mice are prevented by ERK inhibition. PloS one. 2010;5(10):e13604.

20. He WA, Berardi E, Cardillo VM, Acharyya S, Aulino P, Thomas-Ahner J, et al. NF-κB–mediated Pax7 dysregulation in the muscle microenvironment promotes cancer cachexia. The J Clin Invest. 2013;123(11):4821-35.

21. Hettmer S, Wagers AJ. Muscling in: Uncovering the origins of rhabdomyosarcoma. Nat Med. 2010;16(2):171-3.

22. Karalaki M, Fili S, Philippou A, Koutsilieris M. Muscle regeneration: cellular and molecular events. In vivo (Athens, Greece). 2009;23(5):779-96.

23. Attaix D, Ventadour S, Codran A, Bechet D, Taillandier D, Combaret L. The ubiquitin-proteasome system and skeletal muscle wasting. Essays Biochem. 2005;41:173-86.

24. Bodine SC, Baehr LM. Skeletal muscle atrophy and the E3 ubiquitin ligases MuRF1 and MAFbx/atrogin-1. Am J Physiol Endocrinol Metab. 2014;307(6):E469-E84.

25. Rom O, Reznick AZ. The role of E3 ubiquitin-ligases MuRF-1 and MAFbx in loss of skeletal muscle mass. Free Radic Biol Med. 2016;98:218-30.

26. Kobayashi S. Choose Delicately and Reuse Adequately: The Newly Revealed Process of Autophagy. Biol Pharm Bull. 2015;38(8):1098-103.

27. Chang YY, Neufeld TP. An Atg1/Atg13 complex with multiple roles in TOR-mediated autophagy regulation. Mol Biol Cell. 2009;20(7):2004-14.

28. He C, Klionsky DJ. Regulation Mechanisms and Signaling Pathways of Autophagy. Annu Rev Genet. 2009;43:67-93.

29. Bonetto A, Aydogdu T, Kunzevitzky N, Guttridge DC, Khuri S, Koniaris LG, et al. STAT3 Activation in Skeletal Muscle Links Muscle Wasting and the Acute Phase Response in Cancer Cachexia. PloS one. 2011;6(7):e22538.

30. Gao S, Carson JA. Lewis lung carcinoma regulation of mechanical stretch-induced protein synthesis in cultured myotubes. Am J Physiol Cell Physiol. 2016;310(1):C66-79.

31. Zhang G, Jin B, Li YP. C/EBPbeta mediates tumour-induced ubiquitin ligase atrogin1/MAFbx upregulation and muscle wasting. EMBO J. 2011;30(20):4323-35.

32. Gasier HG, Riechman SE, Wiggs MP, Previs SF, Fluckey JD. A comparison of 2H2O and phenylalanine flooding dose to investigate muscle protein synthesis with acute exercise in rats. Am J Physiol Endocrinol Metab. 2009;297(1):E252-9.

33. Nilsson MI, Dobson JP, Greene NP, Wiggs MP, Shimkus KL, Wudeck EV, et al. Abnormal protein turnover and anabolic resistance to exercise in sarcopenic obesity. FASEB J 2013;27(10):3905-16.

34. Hudson MB, Smuder AJ, Nelson WB, Wiggs MP, Shimkus KL, Fluckey JD, et al. Partial Support Ventilation and Mitochondrial-Targeted Antioxidants Protect against Ventilator-Induced Decreases in Diaphragm Muscle Protein Synthesis. PloS one. 2015;10(9):e0137693.

35. Nilsson MI, Greene NP, Dobson JP, Wiggs MP, Gasier HG, Macias BR, et al. Insulin resistance syndrome blunts the mitochondrial anabolic response following resistance exercise. Am J Physiol Endocrinol Metab. 2010;299(3):E466-74.

36. Brown JL, Rosa-Caldwell ME, Lee DE, Brown LA, Perry RA, Shimkus KL, et al. PGC-1alpha4 gene expression is suppressed by the IL-6-MEK-ERK 1/2 MAPK signalling axis and altered by resistance exercise, obesity and muscle injury. Acta Physiol (Oxford, England). 2016.

37. Lee DE, Brown JL, Rosa ME, Brown LA, Perry RA, Jr., Wiggs MP, et al. microRNA-16 Is Downregulated During Insulin Resistance and Controls Skeletal Muscle Protein Accretion. J Cell Biochem. 2016;117(8):1775-87.

38. Call JA, Wilson RJ, Laker RC, Zhang M, Kundu M, Yan Z. Ulk1-mediated autophagy plays an essential role in mitochondrial remodeling and functional regeneration of skeletal muscle. Am J Physiol Cell Physiol. 2017;312(6):C724-c32.

39. Lee DE, Brown JL, Rosa-Caldwell ME, Blackwell TA, Perry RA, Jr., Brown LA, et al. Cancer Cachexia-Induced Muscle Atrophy: Evidence for Alterations in microRNAs important for Muscle Size. Physiol Genomics. 2017:physiolgenomics.00006.2017.

40. Jackman RW, Floro J, Yoshimine R, Zitin B, Eiampikul M, El-Jack K, et al. Continuous Release of Tumor-Derived Factors Improves the Modeling of Cachexia in Muscle Cell Culture. Front Physiol. 2017;8:738.

41. Goodman CA, Hornberger TA. Measuring protein synthesis with SUnSET: a valid alternative to traditional techniques? Exerc Sport Sci Rev. 2013;41(2):107-15.

42. Goodman CA, Mabrey DM, Frey JW, Miu MH, Schmidt EK, Pierre P, et al. Novel insights into the regulation of skeletal muscle protein synthesis as revealed by a new nonradioactive in vivo technique. FASEB J. 2011;25(3):1028-39.

43. Buckingham M. Skeletal muscle progenitor cells and the role of Pax genes. C R Biol. 2007;330(6-7):530-3.

44. Pain VM. Initiation of protein synthesis in eukaryotic cells. FEBS. 1996;236(3):747-71.

45. Porter JD, Khanna S, Kaminski HJ, Rao JS, Merriam AP, Richmonds CR, et al. A chronic inflammatory response dominates the skeletal muscle molecular signature in dystrophin-deficient mdx mice. Hum Mol Genet. 2002;11(3):263-72.

46. Wilde JM, Gumucio JP, Grekin JA, Sarver DC, Noah AC, Ruehlmann DG, et al. Inhibition of p38 mitogen-activated protein kinase signaling reduces fibrosis and lipid accumulation after rotator cuff repair. J Shoulder Elbow Surg. 2016;25(9):1501-8.

47. Sandri M, Sandri C, Gilbert A, Skurk C, Calabria E, Picard A, et al. Foxo transcription factors induce the atrophy-related ubiquitin ligase atrogin-1 and cause skeletal muscle atrophy. Cell. 2004;117(3):399-412.

48. Lima M, Sato S, Enos RT, Baynes JW, Carson JA. Development of an UPLC mass spectrometry method for measurement of myofibrillar protein synthesis: application to analysis of murine muscles during cancer cachexia. J Appl Physiol. 2013;114(6):824-8.

49. Mochamat, Cuhls H, Marinova M, Kaasa S, Stieber C, Conrad R, et al. A systematic review on the role of vitamins, minerals, proteins, and other supplements for the treatment of cachexia in cancer: a European Palliative Care Research Centre cachexia project. J Cachexia Sarcopenia Muscle. 2017;8(1):25-39.

50. Pin F, Busquets S, Toledo M, Camperi A, Lopez-Soriano FJ, Costelli P, et al. Combination of exercise training and erythropoietin prevents cancer-induced muscle alterations. Oncotarget. 2015;6(41):43202-15.

51. Kuang S, Gillespie MA, Rudnicki MA. Niche regulation of muscle satellite cell self-renewal and differentiation. Cell Stem Cell. 2008;2(1):22-31.

52. Jackson JR, Mula J, Kirby TJ, Fry CS, Lee JD, Ubele MF, et al. Satellite cell depletion does not inhibit adult skeletal muscle regrowth following unloading-induced atrophy. Am J Physiol Cell Physiol. 2012;303(8):C854-61.

53. Murach KA, Englund DA, Dupont-Versteegden EE, McCarthy JJ, Peterson CA. Myonuclear Domain Flexibility Challenges Rigid Assumptions on Satellite Cell Contribution to Skeletal Muscle Fiber Hypertrophy. Front Physiol. 2018;9:635.

54. Bongers KS, Fox DK, Ebert SM, Kunkel SD, Dyle MC, Bullard SA, et al. Skeletal muscle denervation causes skeletal muscle atrophy through a pathway that involves both Gadd45a and HDAC4. Am J Physiol Endocrinol Metab. 2013;305(7):E907-15.

55. Furlow JD, Watson ML, Waddell DS, Neff ES, Baehr LM, Ross AP, et al. Altered gene expression patterns in muscle ring finger 1 null mice during denervation- and dexamethasone-induced muscle atrophy. Physiol Genomics. 2013;45(23):1168-85.

56. Hyatt JP, Roy RR, Baldwin KM, Edgerton VR. Nerve activity-independent regulation of skeletal muscle atrophy: role of MyoD and myogenin in satellite cells and myonuclei. Am J Physiol Cell Physiol. 2003;285(5):C1161-73.

57. Pennefather P, Quastel DM. Relation between subsynaptic receptor blockade and response to quantal transmitter at the mouse neuromuscular junction. J Gen Physiol. 1981;78(3):313-44.

58. Johns N, Stephens NA, Fearon KC. Muscle wasting in cancer. Int J Biochem Cell Biol 2013;45(10):2215-29.

59. Toledo M, Busquets S, Penna F, Zhou X, Marmonti E, Betancourt A, et al. Complete reversal of muscle wasting in experimental cancer cachexia: Additive effects of activin type II receptor inhibition and beta-2 agonist. Int J Cancer. 2016;138(8):2021-9.

60. Llovera M, Garcia-Martinez C, Lopez-Soriano J, Agell N, Lopez-Soriano FJ, Garcia I, et al. Protein turnover in skeletal muscle of tumour-bearing transgenic mice overexpressing the soluble TNF receptor-1. Cancer Lett. 1998;130(1-2):19-27.

61. Hardee JP, Counts BR, Gao S, VanderVeen BN, Fix DK, Koh HJ, et al. Inflammatory signalling regulates eccentric contraction-induced protein synthesis in cachectic skeletal muscle. J Cachexia Sarcopenia Muscle. 2018;9(2):369-83.

62. White JP, Puppa MJ, Sato S, Gao S, Price RL, Baynes JW, et al. IL-6 regulation on skeletal muscle mitochondrial remodeling during cancer cachexia in the ApcMin/+ mouse. Skeletal Muscle. 2012;2:14.

63. Schiaffino S, Dyar KA, Ciciliot S, Blaauw B, Sandri M. Mechanisms regulating skeletal muscle growth and atrophy. FEBS J. 2013;280(17):4294-314.

64. Liu Y, Wang X, Leng W, Pi D, Tu Z, Zhu H, et al. Aspartate inhibits LPS-induced MAFbx and MuRF1 expression in skeletal muscle in weaned pigs by regulating Akt, AMPKalpha and FOXO1. J Innate Immun. 2017;23(1):34-43.

65. Levine S, Biswas C, Dierov J, Barsotti R, Shrager JB, Nguyen T, et al. Increased proteolysis, myosin depletion, and atrophic AKT-FOXO signaling in human diaphragm disuse. Am J Respir Crit Care Med. 2011;183(4):483-90.

66. Wynn TA. Cellular and molecular mechanisms of fibrosis. Am J Pathol. 2008;214(2):199-210.

67. Shefer G, Oron U, Irintchev A, Wernig A, Halevy O. Skeletal muscle cell activation by low-energy laser irradiation: a role for the MAPK/ERK pathway. J Cell Physiol. 2001;187(1):73-80.

68. Ding H, Zhang G, Sin KW, Liu Z, Lin RK, Li M, et al. Activin A induces skeletal muscle catabolism via p38beta mitogen-activated protein kinase. J Cachexia Sarcopenia Muscle. 2017;8(2):202-12.

69. Quan-Jun Y, Yan H, Yong-Long H, Li-Li W, Jie L, Jin-Lu H, et al. Selumetinib Attenuates Skeletal Muscle Wasting in Murine Cachexia Model through ERK Inhibition and AKT Activation. Mol Cancer Ther. 2017;16(2):334-43.

70. Li YP, Chen Y, John J, Moylan J, Jin B, Mann DL, et al. TNF-alpha acts via p38 MAPK to stimulate expression of the ubiquitin ligase atrogin1/MAFbx in skeletal muscle. FASEB J 2005;19(3):362-70.

71. Bowen TS, Adams V, Werner S, Fischer T, Vinke P, Brogger MN, et al. Small-molecule inhibition of MuRF1 attenuates skeletal muscle atrophy and dysfunction in cardiac cachexia. J Cachexia Sarcopenia Muscle. 2017;8(6):939-53.

72. Penna F, Bonetto A, Aversa Z, Minero VG, Rossi Fanelli F, Costelli P, et al. Effect of the specific proteasome inhibitor bortezomib on cancer-related muscle wasting. J Cachexia Sarcopenia Muscle. 2016;7(3):345-54.

73. Conte E, Camerino GM, Mele A, De Bellis M, Pierno S, Rana F, et al. Growth hormone secretagogues prevent dysregulation of skeletal muscle calcium homeostasis in a rat model of cisplatin-induced cachexia. J Cachexia Sarcopenia Muscle. 2017;8(3):386-404.

74. Stewart Coats AJ, Ho GF, Prabhash K, von Haehling S, Tilson J, Brown R, et al. Espindolol for the treatment and prevention of cachexia in patients with stage III/IV non-small cell lung cancer or colorectal cancer: a randomized, double-blind, placebo-controlled, international multicentre phase II study (the ACT-ONE trial). J Cachexia Sarcopenia Muscle. 2016;7(3):355-65.

75. Toledo M, Penna F, Oliva F, Luque M, Betancourt A, Marmonti E, et al. A multifactorial anti-cachectic approach for cancer cachexia in a rat model undergoing chemotherapy. J Cachexia Sarcopenia Muscle. 2016;7(1):48-59.

76. Molinari F, Pin F, Gorini S, Chiandotto S, Pontecorvo L, Penna F, et al. The mitochondrial metabolic reprogramming agent trimetazidine as an 'exercise mimetic' in cachectic C26-bearing mice. J Cachexia Sarcopenia Muscle. 2017;8(6):954-73.

77. Barazzoni R, Gortan Cappellari G, Palus S, Vinci P, Ruozi G, Zanetti M, et al. Acylated ghrelin treatment normalizes skeletal muscle mitochondrial oxidative capacity and AKT phosphorylation in rat chronic heart failure. J Cachexia Sarcopenia Muscle. 2017;8(6):991-8.

78. von Haehling S, Morley JE, Coats AJS, Anker SD. Ethical guidelines for publishing in the journal of cachexia, sarcopenia and muscle: update 2017. J Cachexia Sarcopenia Muscle. 2017;8(6):1081-3.

Figure Legends

Figure 1. Cross sectional area throughout the progression of cancer-cachexia. A: Hematoxylin and Eosin staining sample images (scale 50 μM). B. Mean CSA of TA muscle fibers throughout the progression of cancer-cachexia. C. Histogram of fiber sizes throughout the progression of cancer-cachexia. N of 7-8 was utilized for each group. Lettering denotes statistical significance (means that do not share the same letter are statistically different) at an alpha set at $p<0.05$.

Figure 2. Satellite cell and myogenic markers are impaired throughout the development of cachexia. A. *Pax7* mRNA content throughout the progression of cancer-cachexia. *MyoD* mRNA content throughout the progression of cancer-cachexia. *CyclinD1* content throughout the progression of cancer-cachexia. *MyoG* content throughout the progression of cancer-cachexia. N of 7-8 was utilized for each group. Lettering denotes statistical significance (means that do not share the same letter are statistically different) at an alpha set at $p<0.05$.

Figure 3. Protein synthesis throughout the progression of cancer-cachexia. A. Mixed FSR throughout the progression of cancer-cachexia. B. Myofibrilar FSR throughout the progression of cancer-cachexia. C. AKT phosphorylation relative to total protein content. Deptor protein content throughout the progression or cancer-cachexia. 4EBP1 phosphorylation relative to total protein content. p70s6k phosphorylation relative to total protein content. D. Sample images for immunoblot analysis. N of 7-8 was utilized for each group. Lettering denotes statistical

significance (means that do not share the same letter are statistically different) at an alpha set at $p<0.05$.

Figure 4. Protein breakdown throughout the progression of cancer-cachexia. A. Protein ubiquitination throughout the progression of cancer-cachexia. FOXO1 protein content throughout the progression of cancer-cachexia. Phosphorylation of FOXO1 relative to total protein content throughout the progression of cancer-cachexia. B. *Atrogin1* mRNA content throughout the progression of cancer-cachexia. B. *MuRF1* mRNA content throughout the progression of cancer-cachexia. C. Beclin1 protein content throughout the progression of cancer-cachexia. C. Total LC3 protein content throughout the progression of cancer-cachexia. C. LC3 II/I ratio throughout the progression of cancer-cachexia. C. p62 protein content throughout the progression of cancer-cachexia. D. Representative immunoblot images. N of 7-8 was utilized for each group. Lettering denotes statistical significance (means that do not share the same letter are statistically different) at an alpha set at $p<0.05$.

Figure 5. Apoptosis throughout the progression of cancer-cachexia. A. Percent TUNEL + nuclei throughout the progression of cancer-cachexia. B. Total caspase 3 protein content throughout the progression of cancer-cachexia. C. Sample images for the TUNEL assay including a positive control image. D. Representative immunoblot images. N of 7-8 per group was utilized. Lettering denotes statistical significance (means that do not share the same letter are statistically different) at an alpha set at $p<0.05$.

Figure 6. MAPK signaling throughout the progression of cancer-cachexia. A. ERK MAPK phosphorylation relative to total protein content. B. p38 MAPK phosphorylation relative to total protein content. C. Representative immunoblot images. N of 7-8 per group was utilized. Lettering denotes statistical significance (means that do not share the same letter are statistically different) at an alpha set at $p<0.05$.

Figure 7. Inhibition of ERK-MAPK does not protect against LCM mediated loss of myotube diameter despite promoting protein synthesis. A: Myotube diameter analysis of control media+vehicle, control media+PD98059, LCM+vehicle and LCM+PD98059. B. ERK MAPK phosphorylation relative to total protein content following 18 hours of control media+vehicle, control media+PD98059, LCM+vehicle and LCM+PD98059 treatment. C: Puromycin incorporation for groups control media+vehicle, control media+PD98059, LCM+vehicle and LCM+PD98059 after 30 minutes puromycin treatment following 18 hours of treatments. D: Protein ubiquitination following 18 hours of control media+vehicle, control media+PD98059, LCM+vehicle and LCM+PD98059 treatment. E. Protein content of p-4EBP1 relative to total 4EBP1, Deptor, p-FOXO3 relative to total FOXO3 and p-FOXO1 content relative to total FOXO1 following 18 hours of control media+vehicle, control media+PD98059, LCM+vehicle and LCM+PD98059 treatment. F. Atrogin-1 and MuRF-1 mRNA content following 18 hours of control media+vehicle, control media+PD98059, LCM+vehicle and LCM+PD98059 treatment. All measured in C2C12 myotubes and normalized to and Ponceau S. Data are mean ± SEM. G: Representative micrograph and immunoblot images for each protein of interest taken in order

from same membrane. N of 6 was utilized for each group. Lettering denotes statistical significance (means that do not share the same letter are statistically different) at an alpha set at $p<0.05$. **ME indicates statistical Main Effect of indicated factor(s).**

Figure 8. Inhibition of p38 MAPK partially protects against LCM-Mediated Loss of Myotube Diameter. A: Myotube diameter analysis of control media+vehicle, control media+SB202190, LCM+vehicle and LCM+SB202190. B. MAPKAPK-2 phosphorylation relative to total protein content following 18 hours of treatments. C: Puromycin incorporated for groups control media+vehicle, control media+SB202190, LCM+vehicle and LCM+SB202190 after 30 minutes puromycin treatment following 18 hours of treatments. D: Protein content of ubiquitin following 18 hours of control media+vehicle, control media+SB202190, LCM+vehicle or LCM+SB202190 treatment. E. Protein content of p-4EBP1 relative to total 4EBP1, Deptor, p-FOXO3 relative to total FOXO3 and p-FOXO1 content relative to total FOXO1 following 18 hours of control media+vehicle, control media+SB202190, LCM+vehicle or LCM+SB202190 treatment. F. Atrogin-1 and MuRF-1 mRNA content following 18 hours of control media+vehicle, control media+SB202190, LCM+vehicle or LCM+SB202190 treatment. All measured in C2C12 myotubes and normalized to and Ponceau S. Data are mean ± SEM. G: Representative micrographs and immunoblot images for each protein of interest taken in order from same membrane. N of 6 was utilized for each group. Lettering denotes statistical

significance (means that do not share the same letter are statistically different) at an alpha set at $p<0.05$. **ME indicates statistical Main Effect of indicated factor(s).**

Figure S1. Denervation markers throughout the progression of cancer-cachexia. A. AchR α mRNA content throughout the progression of cancer-cachexia. B. AchR δ mRNA content throughout the progression of cancer-cachexia. C. AchR ε mRNA content throughout the progression of cancer-cachexia. D. Gad45A mRNA content throughout the progression of cancer-cachexia. E. Runx1 mRNA content throughout the progression of cancer-cachexia. F. Mus A mRNA content throughout the progression of cancer-cachexia. N of 7-8 was utilized for each group. Lettering denotes statistical significance at an alpha set at $p<0.05$.

Figure 1

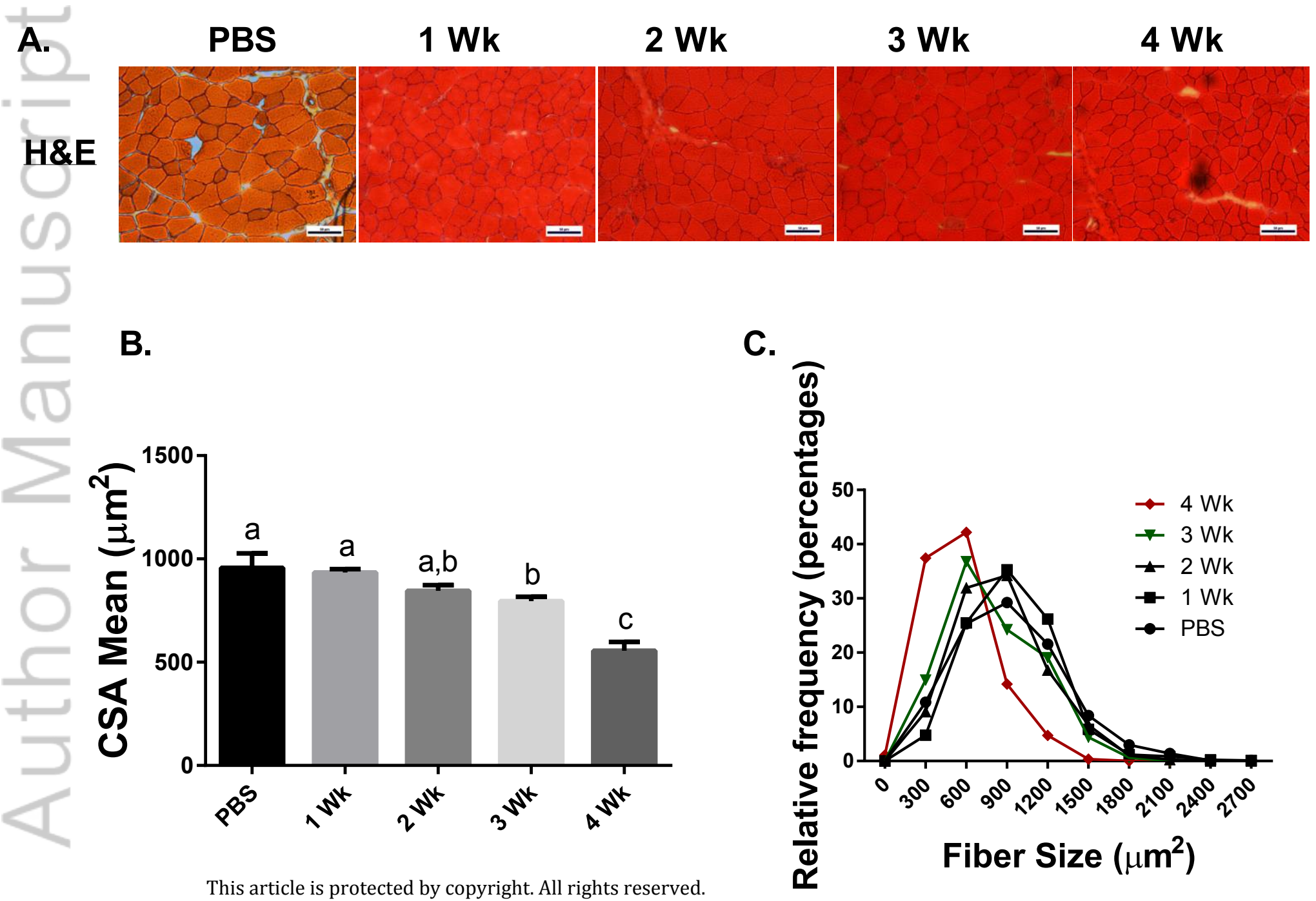

Figure 2

A.

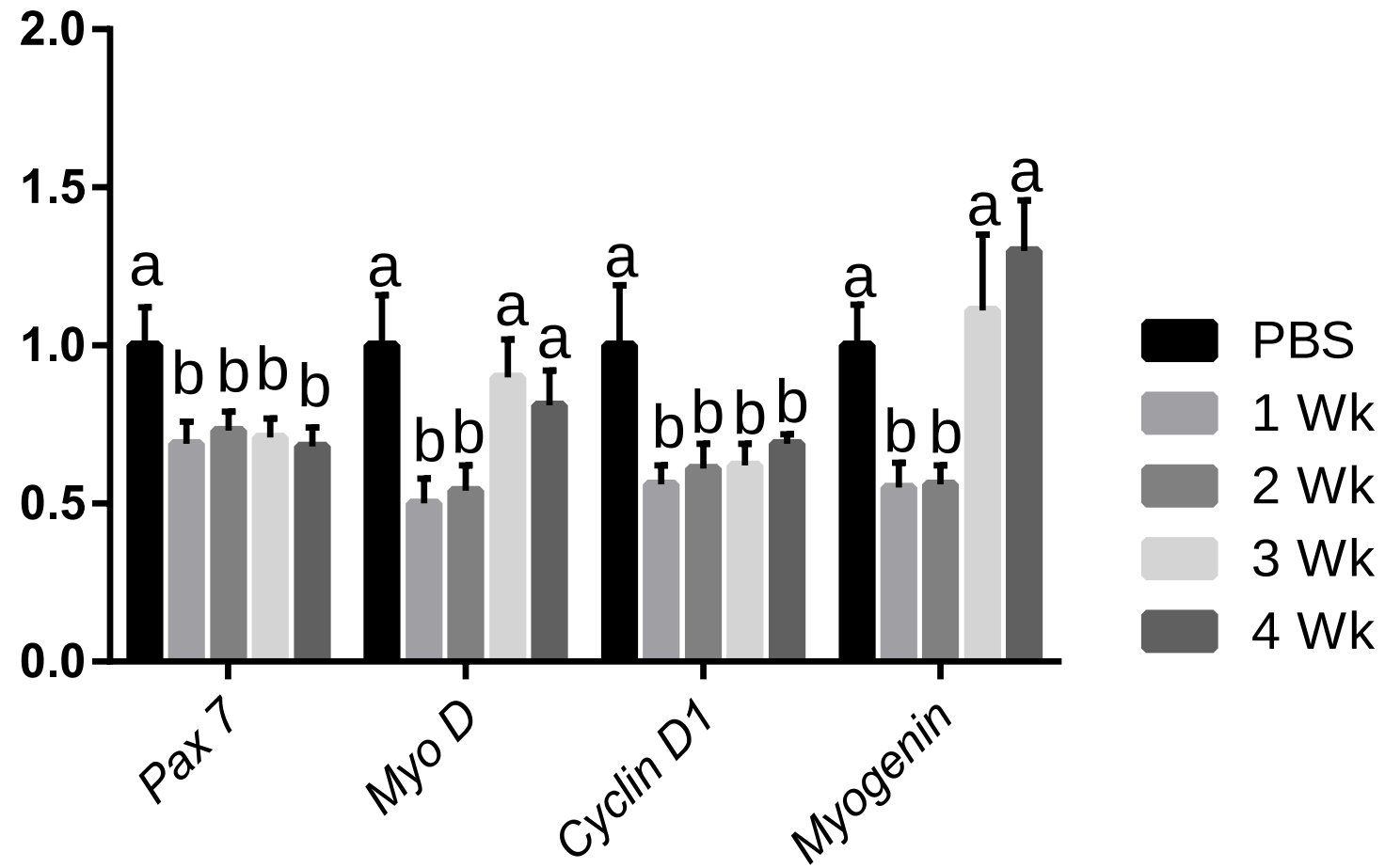

Figure 3

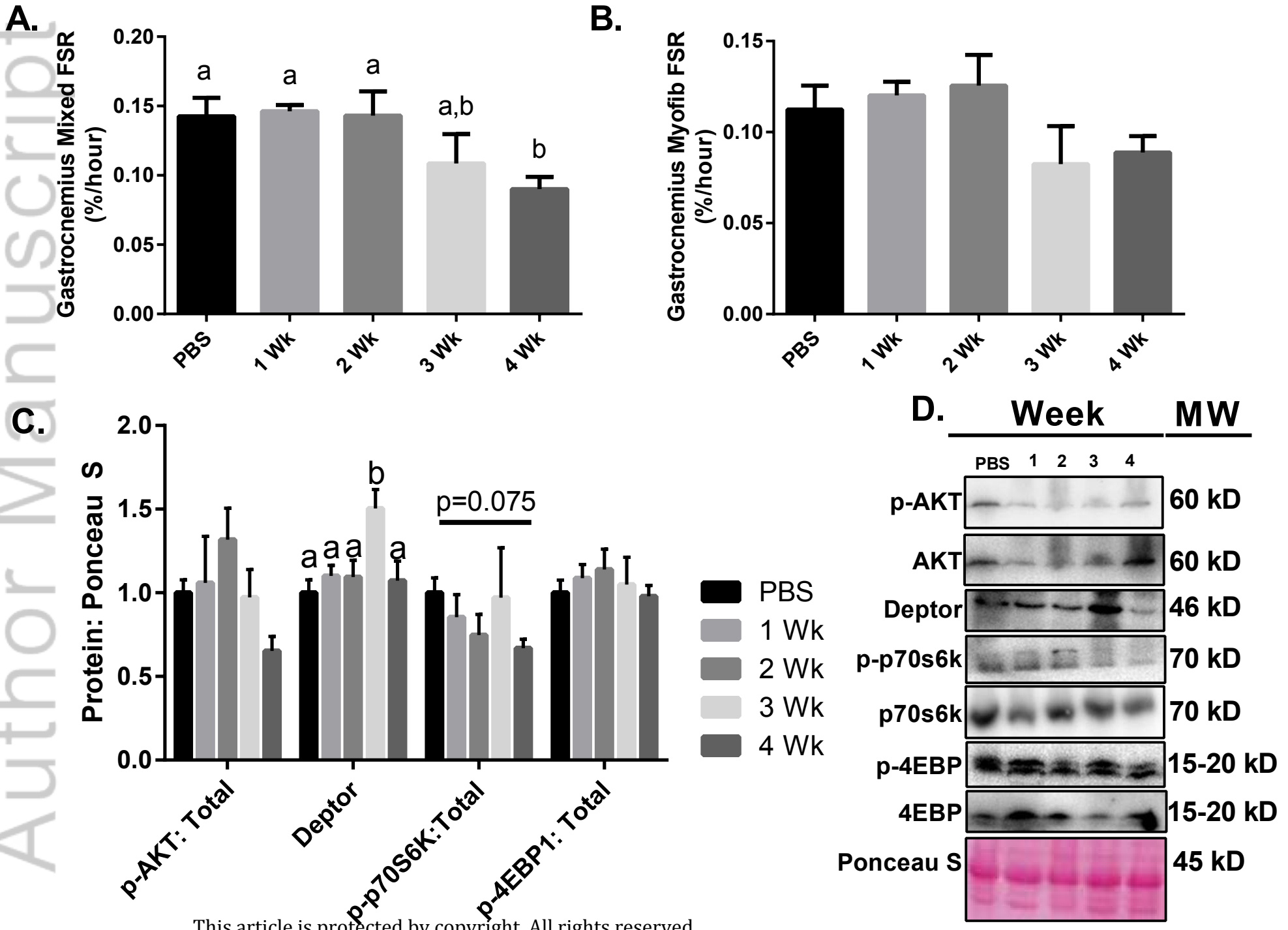

Figure 4

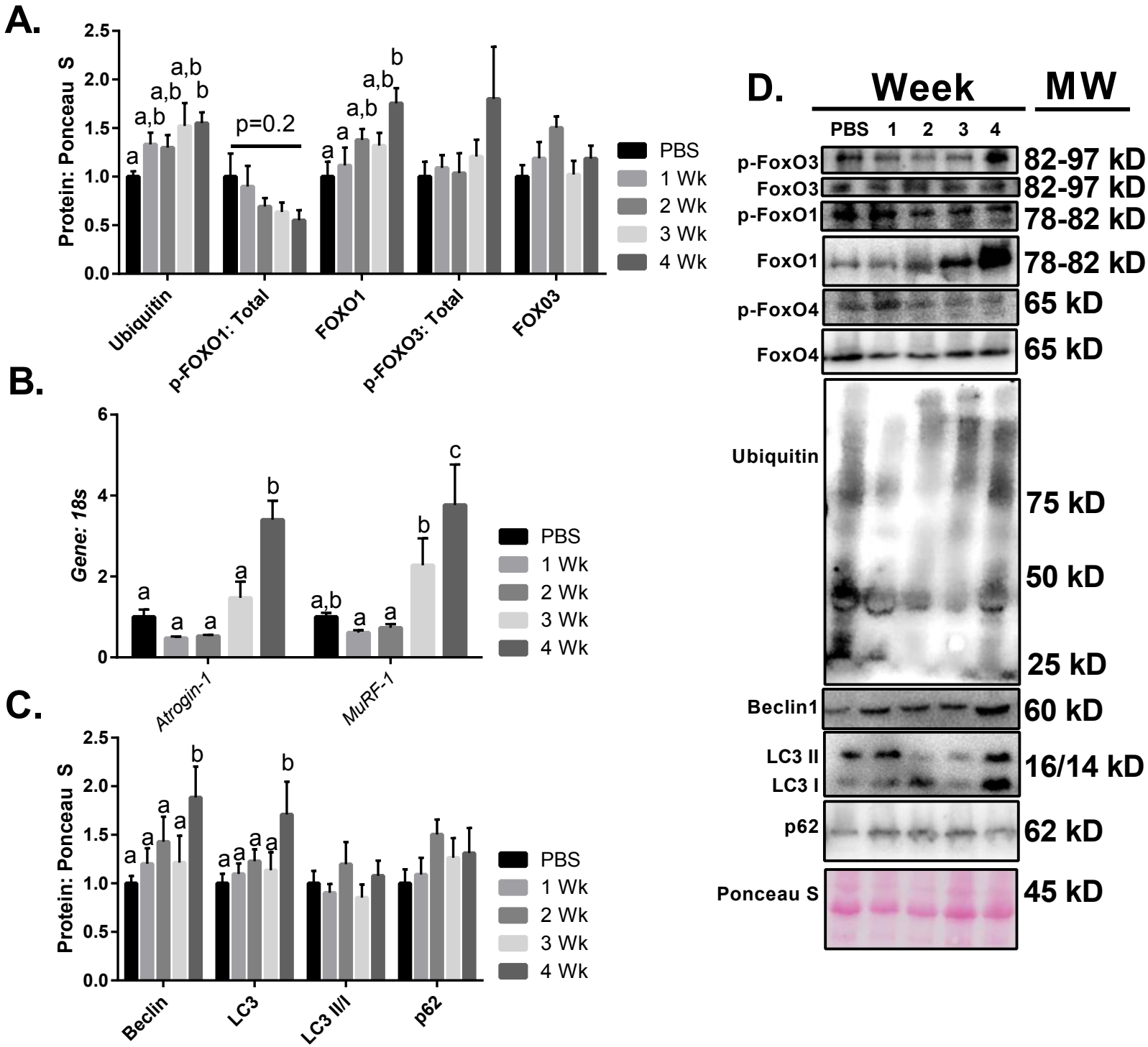

Figure 5

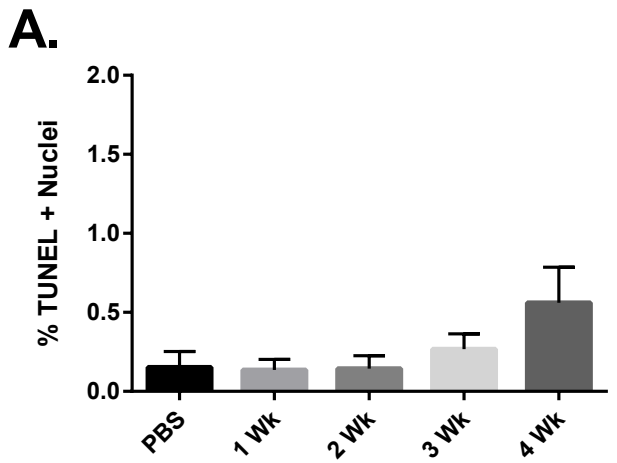

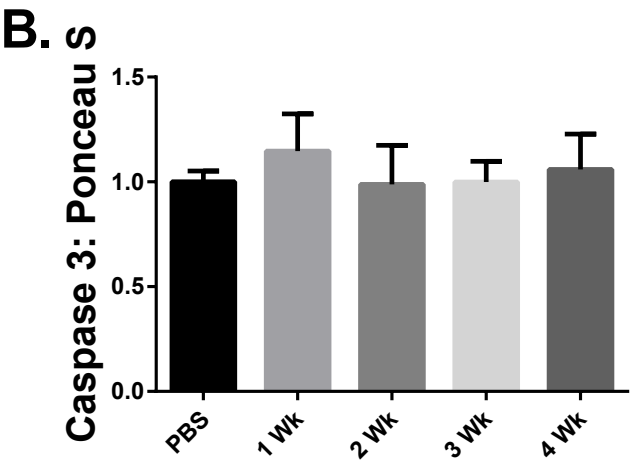

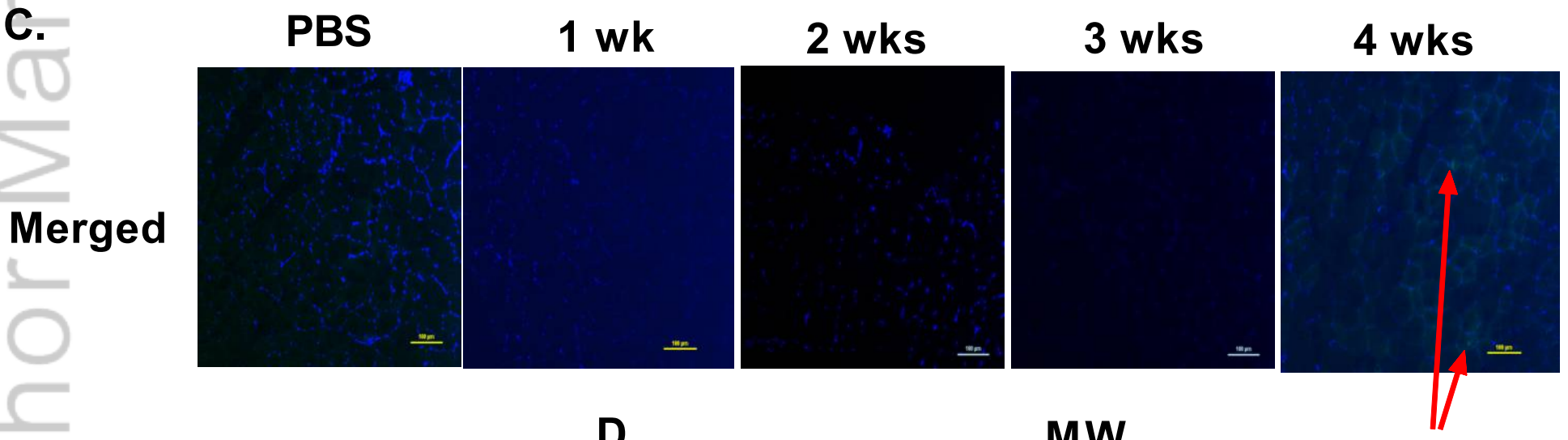

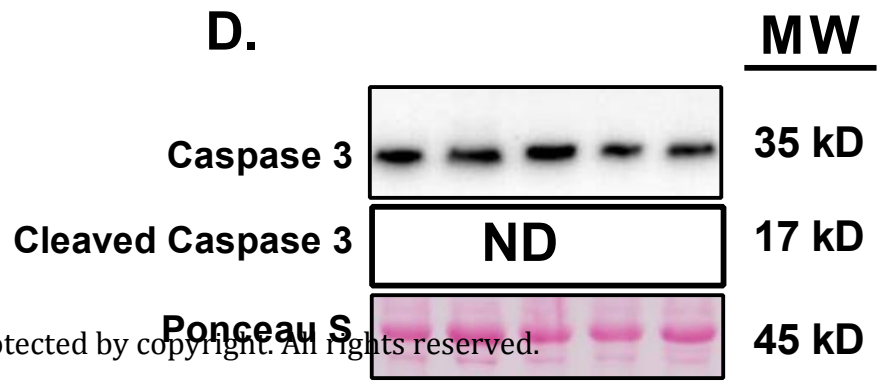

Figure 6

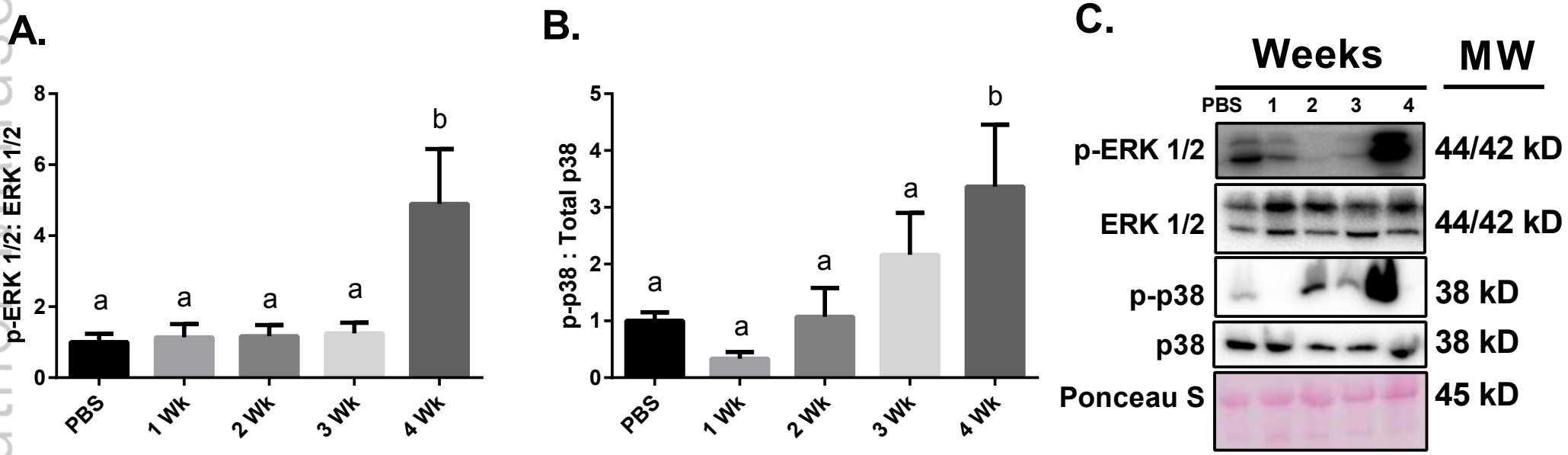

Figure 7

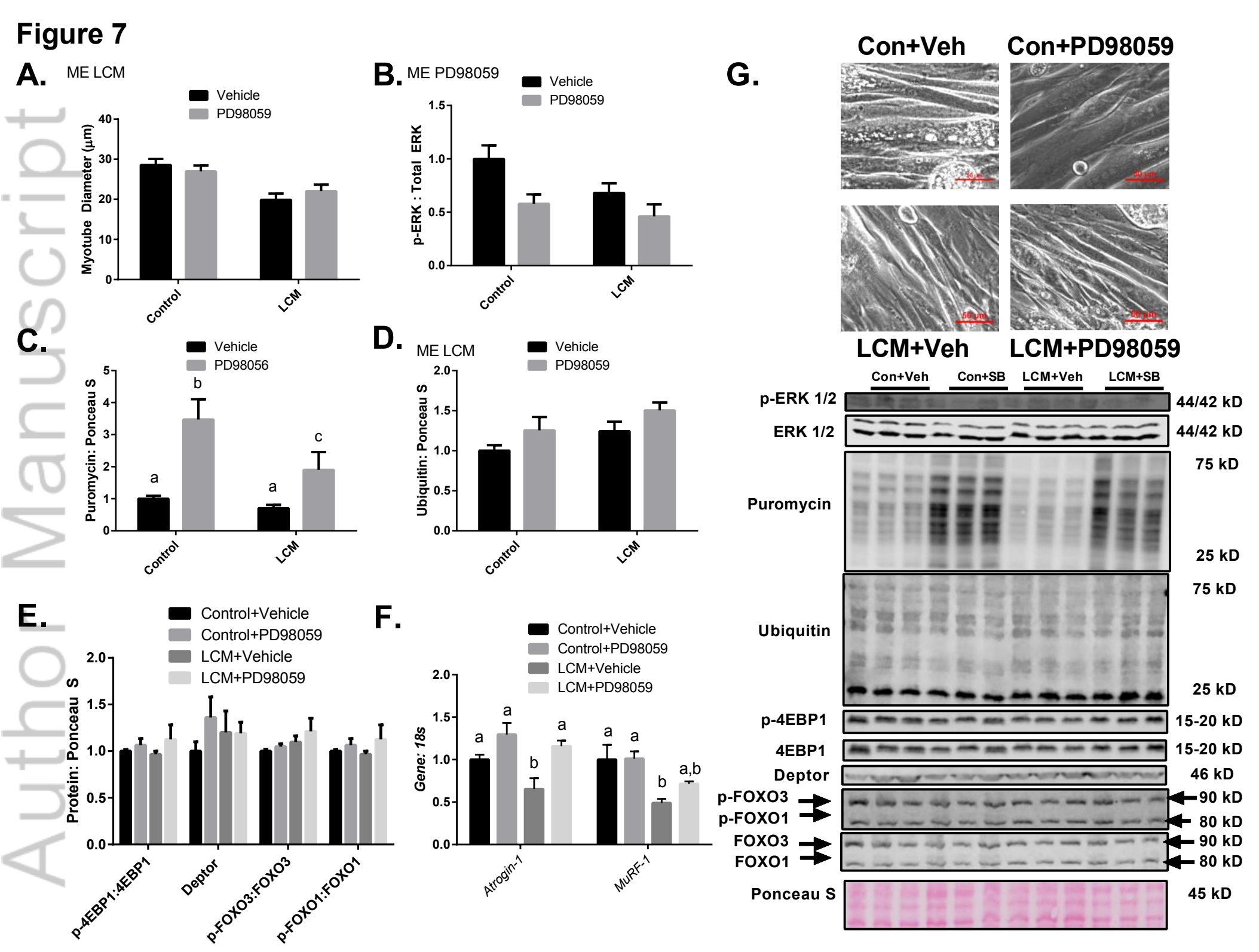

Figure 8